Hindawi
Shock and Vibration
Volume 2021, Article ID 9930221, 15 pages
https://doi.org/10.1155/2021/9930221

*Research Article*

# Stability Analysis and Fracture Patterns of Hard Main Roof in Longwall Top Coal Caving with Large Mining Height

**Jinkai Liu,[1,2] Chunyuan Li,[1,3] Yaoyu Shi,[1] and Yong Zhang[1]**

[1]*Beijing Key Laboratory for Precise Mining of Intergrown Energy and Resources, China University of Mining and Technology (Beijing), Beijing 100083, China*
[2]*China Chemical Mingda Holding Group Co., Ltd., Beijing 100013, China*
[3]*Deep Mining and Rock Burst Research Institute, China Academy of Coal Science, Beijing 100013, China*

Correspondence should be addressed to Chunyuan Li; lcy6055@163.com

Received 16 March 2021; Accepted 23 April 2021; Published 4 May 2021

Academic Editor: Gong-Da Wang



In order to study the fracture patterns of hard main roof in longwall top coal caving (LTCC) with large mining height, a two-dimensional physical similarity model was created to simulate the mining process of No. 8100 large mining height face in Tongxin coal mine, China. The results show that there are three positions of broken line in hard main roof presented with the advance of longwall face, and the underground pressure induced by hard main roof fracturing presents the effect of superposition of large and small periods. It is found that there are two fracture patterns of main roof during the mining process: composite structure of lower cantilever beam and upper voussoir beam with hard main roof and composite structure instability of lower and upper voussoir beam with hard main roof. The underground pressure induced by these two fracture patterns is also analyzed by building mechanical models. In the end, the hydraulic fracture technique is introduced to presplit the main roof and weaken the effect of dynamic loads induced by composite structures instability.

## 1. Introduction

Roof movement, pressure distribution, and control are always the research hotpot of longwall mining [1, 2]. Compared with fully mechanized mining, the movement and structure of overlying strata in longwall top coal caving (LTCC) present some new characteristics [3]. Therefore, it is necessary to discuss the migration law and structural characteristics of overlying strata in combination with the technical characteristics of LTCC mining.

In the past 30 years, the LTCC mining has been widely used in China. Based on rich engineering practice, scholars have conducted a lot of research on the structural characteristics and movement law of roof overburden under different mining technologies [4–7]. For the LTCC mining with large mining height, the movement and structure of overlying strata also have new features due to the larger mining height. Yan and colleagues established a constitutive model using the theory of material mechanics, simplified the roof overburden structure of LTCC mining as "combined cantilever with hinged rock beam structure," and revealed that the instability of the upper hinged rock beam structure and the fracture instability of the lower combined cantilever beam in the longwall face caused the large and small periods of roof overburden structure, respectively [8, 9]. Li and colleagues explained that the overburden strata of LTCC face form the "upper voussoir beam + lower inverted step composite cantilever structure," and the instability of the upper main roof voussoir beam structure will form a short period of strong dynamic loads weighting [10, 11]. By investigating the roof structure evolution in LTCC mining of extra-thick coal seam in Datong mine area, Shanxi province in China, Yu and colleagues put forward the concepts of near-field key stratum (key stratum at low position) and far-field key stratum (key layer at high position far away from coal seam) [12].

Generally, the methods for studying the roof movement consist of four categories: mechanics analysis, similar material simulation, the numerical simulation method, and field

monitoring [13–15]. For the theoretical analysis, the strata in longwall face are generally regarded as a continuous medium. According to the approximate continuous medium characteristics before fracture and discontinuous medium characteristics after fracture, the strata before fracture are regarded as beams or plates and analyzed by material mechanics and plate theory, such as key stratum theory [16], and the strata after fracture are simplified as rock beams composed of rock blocks, such as voussoir beam theory and transferred rock beam theory, analyzed by structural statics analysis [17]. The key of theoretical analysis is the simplification of rock medium or structure. Similar material simulation is widely used in the study of strata control, most of which are plane stress models. This method can directly show the movement and failure of overlying strata in the mining process. However, the mechanical parameters of the simulated strata and the model creating have great influence on the results; it is difficult to eliminate the lateral deformation and drying shrinkage deformation errors of the two-dimensional model, which is generally used to obtain qualitative results [18]. Numerical simulation is generally based on continuous and discontinuous medium mechanics, mainly including finite element, boundary element, and discrete element. Limited by the numerical model and the value of material constant, it is also generally used to obtain qualitative conclusions [19]. Field monitoring directly reflects the roof movement and underground pressure behavior through the collection of longwall face environment change. The main observation contents include roof displacement and hydraulic support pressure. The observation lags mining, and it is difficult to directly reveal the internal mechanism reflected [20]. Therefore, in engineering practice, these methods are often used to study longwall face problems from different angles, so that to reveal the mechanism and put forward protective measures.

In this study, based on the field observation and similar simulation test results in No. 8100 LTCC face with large mining height, Tongxin coal mine of Shanxi Province, China, the overburden fracture modes of LTCC face with large mining height are studied, the composite structure mechanical models of hard main roof are built, and the stability of the composite structures is also analyzed.

## 2. Fracture Behaviors of Hard Main Roof in LTCC with Large Mining Height

*2.1. Engineering Geology.* The No. 8100 LTCC face equips with the Eickhoff SL-500AC coal mining machine and ZF15000/27.5/42 four-link low-top coal caving support, ZF13000/27.5/42H transition support, and ZTZ20000/30/42 end support, and the roof is handled as caving methods. The minimum roof-control distance is 5655 mm. The No. 8100 face is the first panel in North one zone, the face is 193 m in inclined length, 1755–1762 m in strike length, 3.9 m in cutting height, and 10.23 m in caving coal thickness; the cycle cutting step is 0.8 m, one cut, and one caving; the initial mining stage is about 20 m without top coal caving. The structures of coal seam and roof are relatively complicated. The properties of coal seam and roof are given in Table 1.

It is a huge thick coal seam with a thickness of 11.0–23.64 m, average of 14.13 m. The coal seam contains 5–10 gangue strata, and the lithology is generally kaolin rock, sandy mudstone, and carbon mudstone, occasionally siltstone or fine sandstone, the total thickness of the gangue is 2.75 m, the hardness coefficient of the coal seam is 2–4, the dip angle of Nos. 3–5 coal seam is 1–5°, and the depth of the coal seam is 403–492 m, average of 447.5 m. The immediate roof in No. 8100 longwall face is sandy mudstone, and the main roof is mainly composed of hard rock strata such as medium sandstone, fine sandstone, coarse sandstone, and sandy conglomerates, and the thickness is large. No. 8100 longwall face is located below the overlying Jurassic No. 8, No. 9, and No. 11 coal seam and the goaf of No. 12 and No. 14 coal seam. The distance from the No. 14 coal seam goaf is 175–194 m, and most of the strata are hard rock.

*2.2. Behaviors Induced by Fracture and Instability of Hard Main Roof.* In order to analyze the main roof fracture laws of LTCC with large mining height, from March 15 to May 5, 2018, the underground pressure behavior in No. 8100 longwall face was recorded, as given in Table 2. The main roof weighting interval is shown in Figure 1.

It could be seen in Table 2, as the longwall face advances, the fracture of the hard main roof leads to the coal rib spall, the pressure of supports was unloaded, and even the columns of supports were crushed to damage. The hard roof was difficult to cave, and the pressure of hydraulic supports increased and safety valves of supports opened frequently; the coal rib spalled seriously, the roof subsidence was large, and the sound of blast in coal was constant; the range of the front abutment pressure enlarges, the roof of roadway sinks, the rock mass at floor area was cracked and heaved, and the roof and floor are more severely failure than the two sides of roadway. When the longwall face was advanced at 348.0 m, 409.5 m, and 486.5 m, the fracture of main roof was the most obvious, and the pressure was the largest, which caused the support components serious damage or supports crushing disasters.

From Figure 1, during the 52 days, there were 11 serious weighting; the weighting interval of main roof showed obvious large and small periods. The large period was about 6-7 days, and the weighting interval was 43.0–50.9 m; the small period was about 3–5 days, and the weighting interval was 17.9–34.2 m. The large and small cycles show obvious nesting; generally, the large period includes one or two small periods. In additional, the large-period breakage of main roof can easily cause damage to large-scale coal rib spall, or even hydraulic supports crushed disasters; while small-period breakage of main roof only caused partly hydraulic supports increasing the resistance, safety valves unloading, or partially coal rib spalling. These behaviors indicate that the main roof in No. 8100 face forms various fracture structures, which will affect the underground pressure in the longwall face. According to this situation, we can further study the fracture mechanism of the hard main roof in LTCC with large mining height, which will provide guidance for prevention and control of mining in similar conditions.

Table 1: Physical properties of coal and roof in No. 8100 longwall face.

| Number | | Lithology | Thickness (m) | Volume weight (kg/m3) | Compressive strength (MPa) | Tensile strength (MPa) | Elastic modulus (GPa) | Remark |
|---|---|---|---|---|---|---|---|---|
| Roof | 17 | Sandy conglomerates | 80 | 2520 | 27.0 | 7.9 | 35.2 | Key stratum |
| | 16 | Fine sandstone | 80 | 2650 | 107.8 | 7.9 | 36.0 | Key stratum |
| | 15 | Medium sandstone | 20 | 2500 | 92.6 | 4.2 | 28.6 | |
| | 14 | Fine sandstone | 40 | 2650 | 107.8 | 7.9 | 35.2 | |
| | 13 | Coarse sandstone | 40 | 2700 | 62.3 | 5.2 | 20.0 | |
| | 12 | Fine sandstone | 40 | 2650 | 107.8 | 7.9 | 35.2 | Key stratum |
| | 11 | Siltstone | 16 | 2400 | 40.7 | 4.5 | 23.5 | |
| | 10 | Coarse sandstone | 16 | 2700 | 62.3 | 5.2 | 20.0 | |
| | 9 | Granule conglomerate | 4 | 2600 | 96.5 | 4.3 | 28.7 | |
| | 8 | Fine sandstone | 24 | 2650 | 107.8 | 8.2 | 35.6 | Key stratum |
| | 7 | Medium-grained sandstone | 4 | 2670 | 90.2 | 6.1 | 29.6 | |
| | 6 | Granule conglomerate | 16 | 2600 | 96.5 | 4.3 | 28.4 | |
| | 5 | Coarse sandstone | 8 | 2700 | 62.3 | 4.8 | 20.3 | |
| | 4 | Fine sandstone | 12 | 2650 | 107.8 | 7.8 | 35.5 | Key stratum |
| | 3 | Siltstone | 6 | 2400 | 40.7 | 5.0 | 23.6 | |
| | 2 | Pebble conglomerate | 8 | 2500 | 92.6 | 7.7 | 36.2 | Key stratum |
| | 1 | Sandy mudstone | 4 | 2580 | 18.5 | 5.5 | 18.4 | |
| Coal seam | | 3–5 coal seam | 15 | 1430 | 14.4 | 1.5 | 1.7 | |

Table 2: The underground pressure behaviors in No. 8100 longwall face.

| Date | Advancing distance (m) | Underground pressure behaviors in working face | Weighting interval (m) |
|---|---|---|---|
| March 15 | 224.1 | The weighting strength was large, the resistance of supports increased obviously, the safety valves of columns opened, the columns sunk 100–200 mm, and the coal rib spalled largely. | |
| March 21 | 267.8 | Weighting strength was normal, supports resistance was not obvious, safety valves of columns opened individually, and the sinking of columns was not obvious. The resistance of 59# and 69# supports increased. | 43.7 |
| March 25 | 285.7 | The pressure of 42–82# supports increased to 34–39 MPa, the spalling of coal rib was 0.5–0.8 m, and the safety valves of columns all opened. The spalling depth of coal rib at 2–14# and 90–104# supports was 0.5–1.0 m. | 17.9 |
| March 30 | 305.0 | The resistance of 35–80# supports increased, the pressure was 35–39 MPa, and most of the safety valves were opened. The spalling depth of 85–91# supports was large, and the top coal at 94–111# supports was broken. | 19.3 |
| April 6 | 348.0 | The front extension beams of 45–47# and 54–60# supports deformed 20 pieces, and 4 pieces of guards were damaged; the dumbbell pins of scraper conveyor at 56-57# supports broke 2 pieces. | 43.0 |
| April 9 | 366.2 | The pressure of 22–100# supports increased to 33–38 MPa. Next day, the top coal leaked at 37-38# and 41–43# supports; the top coal at 5–88# supports was fragmentized, and the height of the roof caving was 1.0–2.5 m. | 18.2 |

Table 2: Continued.

| Date | Advancing distance (m) | Underground pressure behaviors in working face | Weighting interval (m) |
|---|---|---|---|
| April 16 | 409.5 | Before the weighting, there was a sound of roof collapse in the goaf; 16 safety valves of 57–75# columns were shot out; the rear tail cylinder of 81# support bursts. During the weighting, all tail windshields were blown over. There were 13 columns of supports damaged in total. | 43.4 |
| April 19 | 435.7 | The rear columns of 69# support were posted down, safety valves of 39–100# supports were mostly opened, the roof at 68, 74, 75, 107, and 108# supports were fragmentized, and the coal rib spalled at 13, 14, 58, 59, and 68# supports. | 26.2 |
| April 26 | 486.5 | The weighting first happened at 59# support; safety valves of 49–70# supports opened about 80%; the columns of 57–65# supports could not stretch. | 50.9 |
| May 1 | 520.7 | The safety valves of 0–72# supports were all opened, and the flex volumes of the columns for 53–66# supports were only 20 mm; the average pressure of 16–72# supports were 36 MPa. | 34.2 |
| May 5 | 539.2 | The resistance of 69–99# supports increased, the maximum pressure was 42 MPa, and the average was 38 MPa; the roof at 45–85# supports was broken; the coal rib spalled slightly at 70–80# supports. | 18.6 |

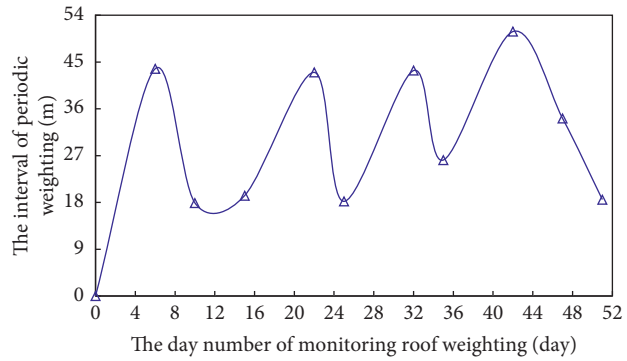


Figure 1: The weighting interval of main roof in full-mechanized coal caving face with large mining height.

## 3. Fracture Patterns of Hard Main Roof in LTCC with Large Mining Height

*3.1. Fracture Patterns and Stress-Strain Curves of Coal and Rock Samples.* In order to study the deformation and fracture of the roof and coal in No. 8100 face, the DNS200 electronic universal testing machine and the XL2158C stress and strain integrated parameter tester (as shown in Figure 2) were used to carry out the stress-strain characters of roof and coal samples. According to ISRM's recommendations for the ratio of height to diameter of the sample for the uniaxial compression test, the samples are a cylinder with a diameter of 25 mm, and the ratio of height to diameter is 2; the loading rate is 0.00167 mm/s. During the test, the axial load and axial displacement data of the samples were recorded by the automatic collection system of the testing machine every 0.1 s until the samples failure.

The typical results of three coal samples (number: C1–C3) and three roof sandstone samples (number: R1–R3) are shown in Figures 3 and 4.

According to Figure 3, the coal occurs as tensile failure. C1 and C3 fracture along the compression surface, and C2 was sheared at about 45°. The roof sandstone presents compressive and torsional structural failure in 45°. In Figure 4, the compressive strength of coal is 15.57 MPa at the maximum and 12.52 MPa at the minimum, and the maximum strain is $0.015 \times 10^{-6}$, and the compressive strength of the roof sandstone is 104.44 MPa at the maximum, 84.06 MPa at the minimum; the maximum strain of the R2 is $0.0215 \times 10^{-6}$. Both coal and roof sandstones are rapidly reduced to residual strength after the peak stress, and the strain has little change and no ductile deformation occurrs. The results show that the strength of Nos. 3–5 coal seams and roof sandstone stratum are large, and they are relatively hard. Under the action of overburden loads, it is easy to induce the instantaneous breaking and instability of top coal and roof strata, which will form an impact on the supports and result in severe underground pressure behaviors.

*3.2. Two-Dimensional Physical Similarity Experiment.* In order to investigate the breaking structure of hard main roof in LTCC face with large mining height, a two-dimensional similar material simulation test was used to carry out the mining process in No. 8100 face, the size of the test platform is 1800 mm × 160 mm × 1200 mm in length × width × height, and a plane stress model was adopted. According to the principle of similar simulation [21–23], the maximum buried depth of No. 8100 longwall face is 492 m, the minimum is 403 m, the simulation set is 440 m, and the model laying height was calculated as 1100 mm; the geometric similarity ratio between the geological model and the similar model is $\alpha_L = 400:1$. According to Table 1, the height of the roof is about 404 m, the thickness of the surface soil stratum is 36 m, and the mixing bulk density ratio of silver sand, cement, gypsum, and other similar materials is $\alpha_\gamma = 1.6:1$. In order to satisfy the motion conditions similar of all corresponding points in the similar model and the geological prototype, the velocity, acceleration, and motion time of the corresponding points of the model and the geological prototype are all in a certain proportion, and the time similarity ratio $\alpha_t = \alpha_L^{1/2}$, so $\alpha_t = 20$.

(a) (b)

Figure 2: Uniaxial compression test devices for coal and rock samples. (a) DNS200 electronic universal testing machine. (b) XL2158C stress and strain integrated parameter tester.

(a) (b)

Figure 3: Fracture patterns of coal and rock samples under uniaxial compression. (a) Coal samples. (b) Sandstone samples.

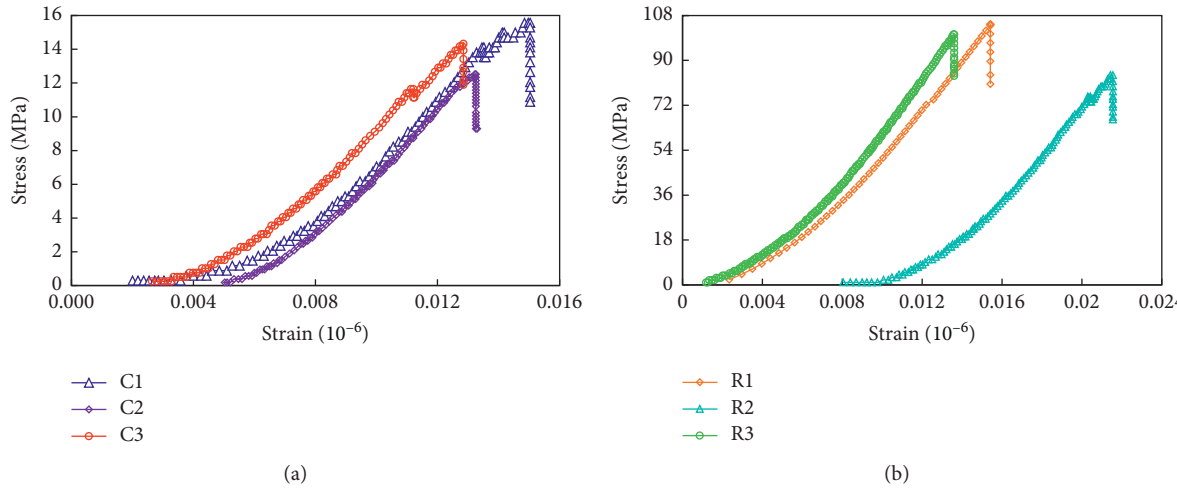


(a) (b)

Figure 4: Stress-strain curves of coal and rock samples under uniaxial compression. (a) Coal samples. (b) Sandstone samples.

The topsoil stratum of the model was simulated with stones with a particle diameter of about 7.5 cm; the similar materials were evenly mixed and compacted manually; mica powder was added between the rock strata to make the model strata clear, and ink was used to mark the coal seams. The ratio and weight of coal and rock strata are given in Table 3.

In order to observe the fracture change and relative motion state of roof, monitor points were arranged on the roof of the model after the model was laid for about five days. A total of 10 rows monitor points were arranged at a vertical distance of 6.25 cm from the top of the coal seam. The grid layout of 10 cm × 10 cm was adopted,as shown in Figure 5. After the model was air-dried for seven days, the coal begun

Table 3: Material mixture ratio and the parameters of the similar model.

| Lithology | Thickness (cm) | Bulk density (g/cm$^3$) | UCS (MPa) | Mixture ratio (sand : cement : plaster) | Total weight (kg) | Sand (kg) | Cement (kg) | Plaster (kg) | Water (kg) |
|---|---|---|---|---|---|---|---|---|---|
| Glutenite | 20 | 1.69 | 0.04 | 13 : 1 : 0 | 9.33 | 8.66 | 0.67 | 0.00 | 0.37 |
| Fine-grained sandstone | 20 | 1.50 | 0.17 | 6 : 7 : 3 | 9.33 | 8.00 | 0.93 | 0.40 | 0.37 |
| Medium conglomerate | 5 | 1.53 | 0.14 | 8 : 7 : 3 | 11.66 | 10.37 | 0.91 | 0.39 | 0.47 |
| Fine-grained sandstone | 10 | 1.58 | 0.17 | 6 : 7 : 3 | 9.33 | 8.00 | 0.93 | 0.40 | 0.37 |
| Fine-grained sandstone | 10 | 1.69 | 0.10 | 10 : 8 : 2 | 9.33 | 8.48 | 0.68 | 0.17 | 0.37 |
| Fine-grained sandstone | 10 | 1.72 | 0.17 | 6 : 7 : 3 | 9.33 | 8.00 | 0.93 | 0.40 | 0.37 |
| Siltstone | 4 | 1.53 | 0.06 | 10 : 9 : 1 | 9.33 | 8.48 | 0.76 | 0.08 | 0.37 |
| Coarse-grained sandstone | 4 | 1.69 | 0.10 | 10 : 8 : 2 | 9.33 | 8.48 | 0.68 | 0.17 | 0.37 |
| Fine conglomerate | 1 | 1.63 | 0.15 | 8 : 7 : 3 | 4.67 | 4.15 | 0.36 | 0.16 | 0.19 |
| Fine-grained sandstone | 6 | 1.66 | 0.17 | 6 : 7 : 3 | 9.33 | 8.00 | 0.93 | 0.40 | 0.37 |
| Medium-grained sandstone | 1 | 1.67 | 0.14 | 8 : 7 : 3 | 4.67 | 4.15 | 0.36 | 0.16 | 0.19 |
| Fine conglomerate | 4 | 1.63 | 0.15 | 8 : 7 : 3 | 9.33 | 8.29 | 0.73 | 0.31 | 0.37 |
| Coarse-grained sandstone | 2 | 1.69 | 0.10 | 10 : 8 : 2 | 9.33 | 8.48 | 0.68 | 0.17 | 0.37 |
| Fine-grained sandstone | 3 | 1.66 | 0.17 | 6 : 7 : 3 | 7.00 | 6.00 | 0.70 | 0.30 | 0.28 |
| Siltstone | 1.5 | 1.50 | 0.06 | 10 : 9 : 1 | 7.00 | 6.36 | 0.57 | 0.06 | 0.28 |
| Medium conglomerate | 2 | 1.56 | 0.14 | 8 : 7 : 3 | 4.67 | 4.15 | 0.36 | 0.16 | 0.19 |
| Sandy mudstone | 1 | 1.61 | 0.03 | 10 : 1 : 0 | 4.67 | 4.24 | 0.42 | 0.00 | 0.19 |
| 3–5 coal seam | 3.75 | 0.89 | 0.02 | 9 : 8 : 2 | 8.75 | 7.87 | 0.70 | 0.17 | 0.35 |

to excavate, and the high-definition camera was used to continuously observe the fracture change and relative motion state of roof. In order to eliminate the influence of the model boundary, 30 cm boundary coal pillars were left on both sides of the model. Therefore, the section marking started at 30 cm away from the left side of the model, and the mining cycle was 4 cm for 20 minutes.

*3.3. Composite Structures Induced by Hard Main Roof Fracture.* As the longwall face advanced, the immediate roof caved and the main roof fractured. The roof fracture structure pictures at different advance distances are shown in Figure 6.

In Figure 6, when the advance distance of LTCC face was 112 m, the immediate roof collapsed first. When the advance distance was 192 m, the roof collapsed in a large area and the first weighting occurred. When the advance distance was 224 m, the roof fracture extends to the upper strata, and the roof above the support was still complete and has little impact on the support. When the advance distance was 336 m, the roof broken line just extends to the support, and it has an important impact on the support. When the advance distance was 400 m, the roof broke and acted on the support, and the broken line was close to the back of the support. When the advance distance was 432 m, the roof broke again and the fracture

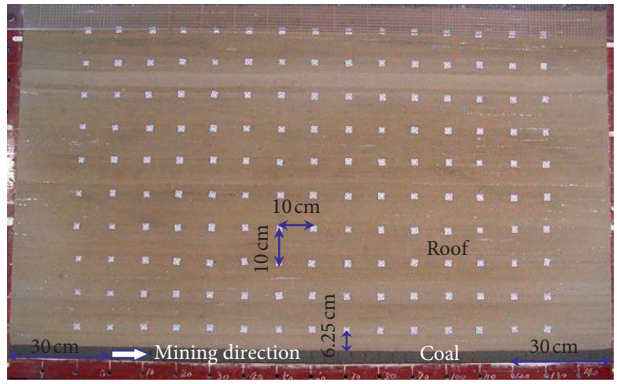


Figure 5: Two-dimensional similar model and the measuring points.

zone in roof further expanded. During the mining process, a total of 5 significant roof breakages were generated, the position of the roof broken line changed with the different advance distances significantly, and their impact and disturbance formed on the support had obvious differences. With the advance of longwall face, the fracture in roof extended to the upper stratum constantly, and the roof fracture structure and the position of the broken line changed.

As the longwall face advanced, the lower stratum of roof fracture formed a cantilever structure as shown in

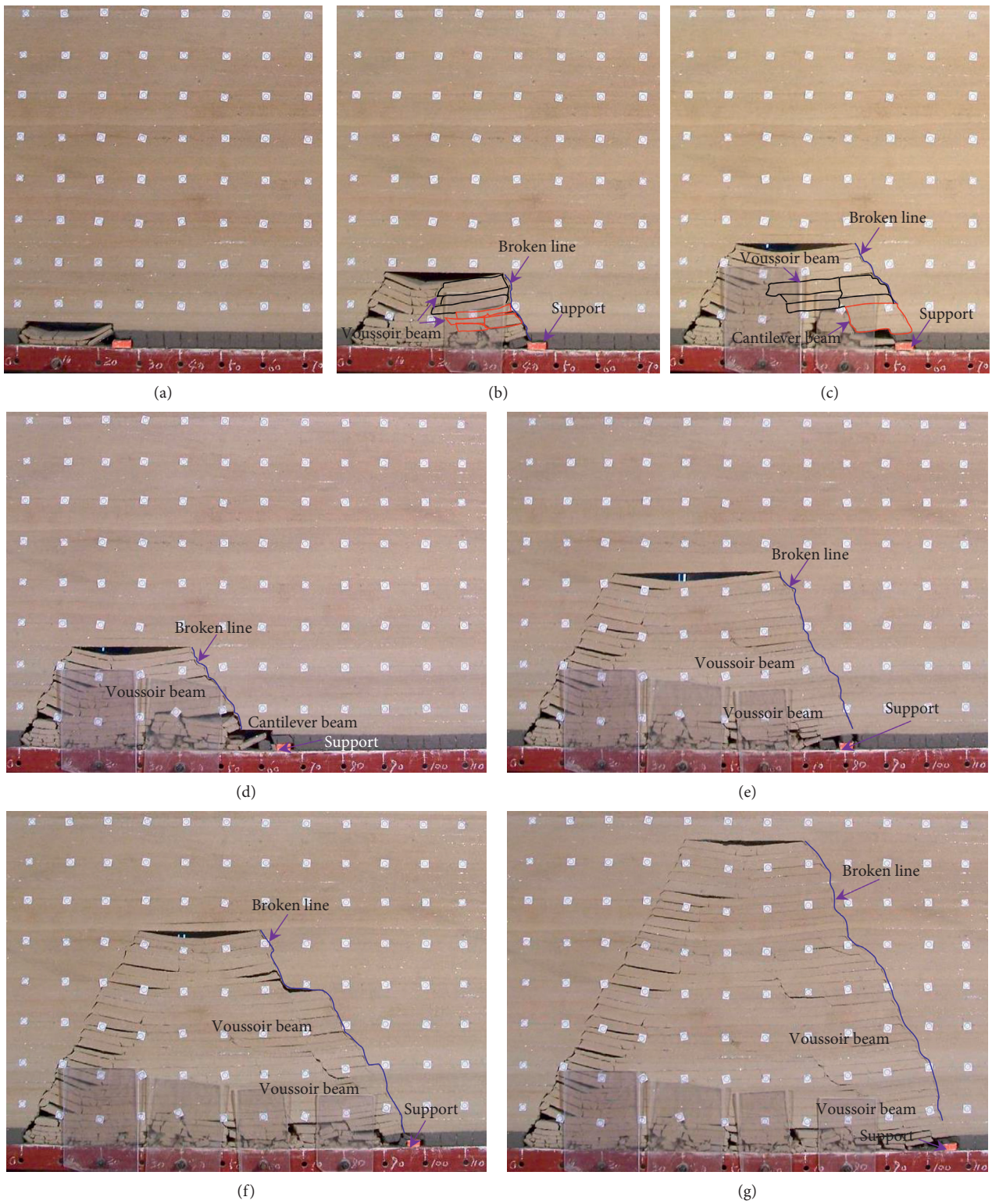


FIGURE 6: Fracture pattern evolution of roof with the advance of LTCC face. (a) 112 m, (b) 192 m, (c) 224 m, (d) 272 m, (e) 336 m, (f) 400 m, and (g) 432 m.

Figures 6(c) and 6(d) and a voussoir beam structure as shown in Figures 6(b), 6(e)–6(g), and the upper rock strata only formed a voussoir beam structure. And the roof of LTCC face was fractured and formed the different composite structures. When the lower stratum fractured as a cantilever structure, the top coal above the supports fractured, and it was still a complete block. The fractured structure of the roof has little effect on the longwall face.

While the lower stratum of roof fracture was in the case of voussoir beam structure, the top coal above the support was mostly broken blocks, the support borne the high loads, and even the top coal in front of the support was caved, as shown in Figures 6(e) and 6(f). With the advance of longwall face, the relative position between the broken line and the support changed. When longwall face advanced 192 m and 272 m, the broken line of roof was behind the support; when longwall face advanced 400 m and 432 m, the broken line was just located above the support; when longwall face advanced 224 m and 336 m, the broken line was located in front of the support.

When the roof broken line was behind the support, the damage of top coal above the support was slight in Figures 6(b) and 6(d). Although a fracture structure had been formed at the goaf, the roof in the goaf broke and the loads were far away from the coal rib and had the least impact on the supports. When the broken line of the roof was directly above or in front of the support, the roof fracture structure in the goaf had the most serious damage to the support, and its damage was related to the span of the lower cantilever beam, the voussoir beam structure, and the upper voussoir beam structure. When the lower rock beam reached the limit span to form an instability structure, the support only borne the lower rock strata and its dynamic loads, and the upper voussoir beam structure did not break simultaneously. The damage of the surrounding rock was relatively weak.

However, compared with the cantilever beam structure, the lower voussoir beam structure was mutually hinged rock blocks. The compression and occlusion of the lower rock blocks in the goaf could easily form long-distance loads transmission, which caused severe disturbance to longwall face, and it would cause a serious underground pressure behavior. While the cantilever beam was a single large block, which was not easy to be squeezed from the block far away from the goaf, the loads transmission was weak, with a slight pressure. When the upper voussoir beam structure fractured, the upper strata structure would drive the lower strata structure to break synchronously, resulting in a serious underground pressure behavior. When the broken line was in front of the support, the top coal caved in a large area. Therefore, the fracture structure of hard main roof and the position of the broken line determine the damage of the surrounding rock and the severity of the pressure in LTCC face with large mining height. In this way, the disaster mechanism of their instability can be analyzed, which would provide a theoretical basis for the control of hard roof.

## 4. Stability Analysis of Composite Structures of Main Roof in LTCC with Large Mining Height

Based on the key stratum theory, the loads and span of hard main roof can be determined, and the instability and hazard mechanism of the two main composite structures could be studied.

*4.1. Composite Structures of Main Roof.* Combining the following equation of the key stratum theory, the position of the key stratum of the main roof could be calculated [24]:

$$\begin{cases} (q_n)_1 = \dfrac{\left(E_1 {h_1}^3 \sum_{i=1}^{n} \gamma_i h_i\right)}{\left(\sum_{i=1}^{n} E_i h_i^3\right)}, \\ q_{n+1} < q_n, \\ l_j < l_{j+1}, \quad j = 1, 2, \ldots, m, \end{cases} \tag{1}$$

where $q_{n+1}$, $q_n$ are the loads on the key strata of the first stratum when $n+1$ and $n$ strata are calculated, respectively, MPa; $E_i$ is the elastic modulus, MPa; $h_i$ is the thickness of the rock stratum, m; $\gamma_i$ is the volume weight, kN/m$^3$; $n$ is the strata controlled by the first stratum to reach $n$ strata; $l_i$ is the fracture span of the hard rock of $j$ strata, m; $m$ is the number of hard rock strata.

Substituting the thickness and basic physical and mechanical parameters of the hard main roof from Table 1 into equation (1), the key strata position in No. 8100 longwall face was calculated and determined, as given in Table 1. The calculated height of the caving zone is shown in the following equation [24]:

$$\begin{aligned} L_n &> \sum h, \\ \sum h &= \frac{M}{K_P - 1}, \end{aligned} \tag{2}$$

where $L_n$ is the distance between the $n^{\text{th}}$ stratum of the roof and the top interface of the coal seam, m; $\sum h$ is the height of the caving zone, m; $M$ is the mining height, m; and $K_P$ is the bulking coefficient, generally taken from 1.3 to 1.5.

The calculation result shows that the height of the roof caving zone in No. 8100 longwall face reaches 30–50 m, and it is extremely difficult for the sandy mudstone to directly fill the mining height. The No. 2 pebble conglomerate and No. 4 fine sandstone stratum near the top interface of the coal seam are extremely hard, which could carry and form a fracture structure by themselves and be arranged in a regular pattern in Figure 6. Although they are within the caving zone, the No. 2 pebble conglomerate and No. 4 fine sandstone stratum could be regarded as the lower key strata. The structural fracture and instability directly determine the severity of the underground pressure behavior, and the stratum located above the height of the caving zone and under the curved subsidence zone could be regarded as the upper key strata. Therefore, the Nos. 8, 12, 16 fine sandstone and No. 17 sandy conglomerates strata in No. 8100 longwall face are the upper hard main roof, and its instability will transfer to the supports through the lower key strata. According to Section 2.3, if the fracture and instability of the composite structures of the lower key strata and the upper key strata are just above the supports or ahead of them, it will easily lead to severe impact loads.

According to Table 2 and Figures 1 and 6, the No. 8100 longwall face has the strong periodic pressure behaviors. The

ultimate fracture span of the key strata could be calculated with the cantilever beam and voussoir beam equation, respectively, as shown in the following equations [17]:

$$\text{Cantilever beam formula: } l_i = h_i\sqrt{\frac{\sigma_i}{3q_i}}, \tag{3}$$

$$\text{Voussoir beam formula: } l_i' = h_i\sqrt{\frac{\sigma_i}{6kq_i}}, \tag{4}$$

where $l_i$ is the fracture span of the $i^{\text{th}}$ strata calculated by the cantilever beam; $l_i'$ is the fracturespan of $i^{\text{th}}$ strata calculated by the simply supported beam; $h_i$ is the thickness of the $i^{\text{th}}$ stratum; $\sigma_i$ is the $i^{\text{th}}$ stratum of rock tensile strength; $q_i$ is the load from the $i^{\text{th}}$ stratum of rock; and $k$ is determined by the fixed or simply supported state of the beam and generally takes 1/2-1/3.

Therefore, the ultimate fracture span of the voussoir beam is about 1.0–1.2 times that of the cantilever beam ($l_i'$ = (1.0–1.2) $l_i$). Substituting the physical and mechanical parameters of the key strata into equations (3) and (4), respectively, the limit fracture span of key strata of different rock formations could be calculated, as given in Table 4.

According to Table 4, the limit fracture span of the lower key strata is between 24.7 and 39.7 m, it is higher than 37.2 m for the upper key strata, and the limit fracture span of the upper key strata is 17.9 m higher than the maximum value of the lower key strata. Affected by the development of internal joints in the rock, the weighting interval of key strata is often less than the limit fracture span. In Figure 1, the weighting interval of the main roof is 17.9–34.2 m during the small period, and it is higher than 43.0 m during the large period. Comparing theoretical calculations with field measurements, the fracture and instability of the lower key strata resulted in the periodic weighting with the small period and a relatively weak pressure behavior; the fracture and instability of the upper key strata resulted in a severe underground pressure behavior, while the fracture position of the lower key strata determine the instability state of the main roof composite structures.

In Figure 6, it easily forms a cantilever beam structure or a voussoir beam structure in the lower key strata for the large mining height, and the upper key strata are all voussoir beam structure due to rock bulking effects and the support actions of the lower rock strata. It could be generated that the hard main roof in No. 8100 longwall face will form two composite structures of fracture and instability, and they are lower cantilever beam-upper voussoir beam and lower voussoir beam-upper voussoir beam.

*4.2. Lower Cantilever Beam with Upper Voussoir Beam.* When the roof broken line is located above or in front of the supports, the instability of main roof is the most obvious, and it most likely to form serious underground pressure behavior and cause the deformation and damage of the supports. Hence, this disaster situation happens most easily and should be studied. In Figure 6(c), with the advance of longwall face, the span of lower key strata of main roof increases, and the free end gradually produces downward bending deformation. When the roof broken line is just above or in front of the support, the cantilever beam will inevitably break and lose stability, and the cantilever beam will undergo rotational instability under the repeated movement of the supports, as shown in Figure 7(a), which will generate underground pressure behavior.

If only the lower cantilever beam lose stability, the supports just bear the weight of top coal, immediate roof, lower cantilever beam, and the instability loads, and the longwall face only forms a small periodic weighting. Ignoring the acting force between lower key strata, the static loads $Q_s$ of the supports could be calculated according to the following equation [25]:

$$Q_s = \frac{1}{2c}\sum_{i=1}^{j} P_i\left(l_i + h_i\cot\alpha\right) + L_d h_d \gamma_m + L_d h_z \gamma_z, \tag{5}$$

where $c$ is the distance between the supporting acting point and the coal rib, m; $P_i$ is the weight and loads of $i^{\text{th}}$ rock of the lower key strata, kN; $h_i$ and $l_i$ are the thickness and length of lower key strata, m; $\alpha$ is the fracture angle of the rock; $L_d$, $h_d$, and $h_z$ are the control distance of support, top coal thickness, and immediate roof thickness, respectively, m; $\gamma_m$ and $\gamma_z$ are the top coal and immediate roof volume weight, respectively, kN/m$^3$.

Because the lower key strata in No. 8100 longwall face include two key strata of No. 2 pebble conglomerate and No. 4 fine sandstone, their fracture instability includes three types: No. 2 pebble conglomerate, No. 4 fine sandstone failure, or two strata simultaneous fracture. The fracture instability of two strata at the same time has the greatest damage to the surrounding rock, and supports will bear certain dynamic loads due to the rotation or impact of the cantilever beam instability. Generally, only the composite fracture structures and the upper overburden loads controlled by itself are calculated, and the impact loads coefficient on the surrounding rock in longwall face is ignored. $K_{dl}$ can be set as the impact loads coefficient of the lower cantilever beam, and the loads $Q_l$ bore by supports could be expressed as

$$Q_l = K_{dl}B\left[\frac{1}{2c}\sum_{i=1}^{j} P_i\left(l_i + h_i\cot\alpha\right) + L_d h_d \gamma_m + L_d h_z \gamma_z\right], \tag{6}$$

where $B$ is the center distance between two supports, m.

It is assumed that the two key strata of No. 2 pebble conglomerate and No. 4 fine sandstone are both cantilever beam structures, and the weighting interval is the limit fracture span of No. 2 pebble conglomerate, $l_1 = l_2 = 24.7$ m, $P_1$ and $P_2$ are the weight of the two key strata and their controlled loads, respectively; $B = 1.75$ m, $c = 5$ m, $\alpha = 70^\circ$, and $K_{\text{dl}} = 1.0$, and then, substituting the rock mechanics parameters in Table 1 into equation (6), $Q_l = 13779.31$ kN. When $K_{\text{dl}} = 1.09$, $Q_l = 15000$ kN, namely, when $K_{\text{dl}} > 1.09$, the simultaneous instability of cantilever beam structures in the lower key strata could cause overburden loads exceeding the working resistance of supports, which will generate a drastic small periodic weighting.

Table 4: Ultimate fracture span of key stratum in No. 8100 longwall face.

| Seam no. | Lithology of key stratum | Position of key stratum | Ultimate fracture span | | Distance from the coal seam (m) |
|---|---|---|---|---|---|
| | | | Cantilever beam | Voussoir beam | |
| 17 | Glutenite | Upper key strata | 91.4 | 91.4–109.7 | 338.0 |
| 16 | Fine-grained sandstone | | 90.0 | 90.0–108.0 | 258.0 |
| 12 | Fine-grained sandstone | | 55.1 | 55.1–66.1 | 118.0 |
| 8 | Fine-grained sandstone | | 37.2 | 37.2–44.6 | 58.0 |
| 4 | Fine-grained sandstone | Lower key strata | 33.1 | 33.1–39.7 | 18.0 |
| 2 | Medium conglomerate | | 24.7 | 24.7–29.6 | 4.0 |

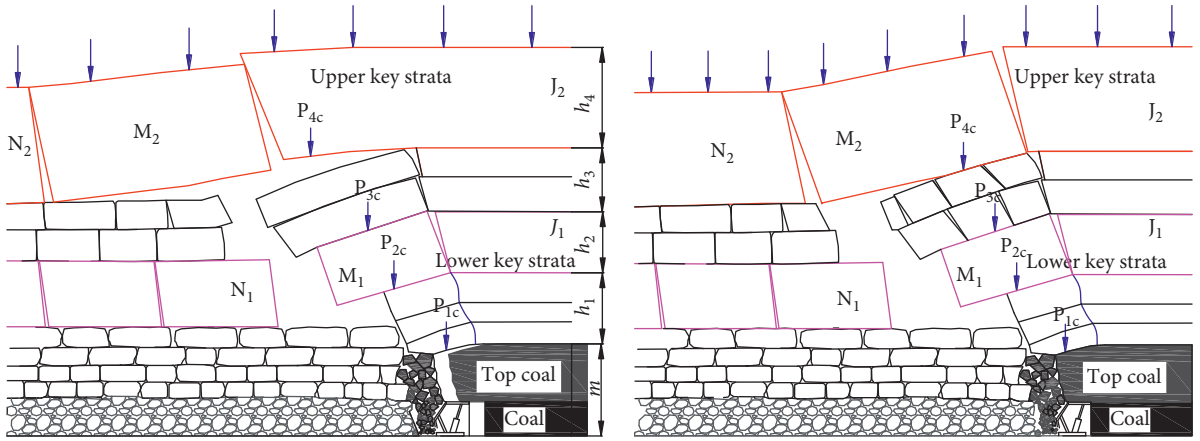


Figure 7: Composite structures of lower cantilever beam and upper voussoir beam with hard main roof. (a) Instability of lower cantilever beam. (b) Synchronous instability of lower and upper structure.

When the upper voussoir beam fractures ahead of the lower cantilever beam, the upper voussoir beam breaks laggingly, and the roof broken line will be located behind the supports. After the coal is mined for a short distance, if the roof broken line is still above the supports, the upper voussoir beam may induce a more serious underground pressure behavior after the lower cantilever beam lose stability, and the lower cantilever beam is simultaneously driving instability again resulting in severe impact loads, as shown in Figure 7(b), which generate a severe small periodic weighting. The initial pressure of the lower cantilever beam is not large, and the pressure will increase significantly in the later stage. If the roof broken line is still above or in front of the supports, the lower key stratum presents a cantilever beam structure and the upper voussoir beam fractures; then, the instability of the upper voussoir beam will drive the lower cantilever beam to instability; thus, the longwall face will form a severe periodic weighting. Therefore, the instability of the voussoir beam structure of the upper key strata on the hard roof will play a key role in the underground pressure behavior. The $Q_c$ acting on the supports after the structure instability could be calculated as [26]

$$Q_c = K_{dc} B \left\{ \frac{1}{2c} \sum_{i=1}^{j} P_i \left(l_i + h_i \cot \alpha\right) + \left[ 2 - \frac{l_{4c} \tan\left(\varphi - \alpha\right)}{2\left(h_{4c} - \delta_{4c}\right)} \right] P_{4c} + L_d h_d \gamma_m + L_d h_z \gamma_z \right\}, \tag{7}$$

where $K_{dc}$ is the impact loads' coefficient for the upper voussoir beam structure instability; $h_{4c}$ is the thickness of key strata in the upper voussoir beam structure, m; $\delta_{4c}$ is the sinking amount of the hinged rock block $M_2$ in the key strata of the upper voussoir beam structure, m; $P_{4c}$ is the load of the hinged rock block and the upper control rock in key strata of the upper voussoir beam structure, kN; $\varphi$ is the friction angle between the hinged rock blocks; and $\alpha$ is the rock fracture angle between the hinged rock blocks.

However, if the upper voussoir beam structure fractures and the lower cantilever beam structures have not reached its periodic fracture span, the upper voussoir beam structures will drive the lower cantilever beam to instability, which could be determined by equation (7), and the lower and upper structures work together to form a large periodic weighting. The fracture span of the lower cantilever beam can be determined by the empirical value of the weighting interval during a small period. The lower cantilever beam

structure has reached its limit fracture span during the upper voussoir beam structure instability, $Q_c > Q_l$. Since the thickness, the span of the upper key strata, and the thickness of the upper rock strata controlled by itself in No. 8100 longwall face are much higher than the lower key strata, the loads of the voussoir beam will be much higher than that of the lower cantilever beam, and the instability of the upper key strata will further drive the instability of the lower cantilever beam. Then, the $Q_c$ acting on the supports will be much greater than $Q_l$, a large periodic weighting will be formed when the upper voussoir beam fractures, and the damage of the surrounding rock will be greater than the lower cantilever beam fracture.

Due to the large space under the lower cantilever, the impact loads coefficient $K_{\mathrm{dl}}$ during the lower cantilever beam instability may be greater than $K_{\mathrm{dc}}$, and the lower cantilever instability during the small period weighting may also induce serious underground pressure behavior. However, its instability loads are less than the upper voussoir beam.

*4.3. Lower Voussoir Beam-Upper Voussoir Beam Structure.* When the roof broken line is above or in front of the supports, the instability of the lower voussoir beam-upper voussoir beam structure is most likely to induce serious underground pressure behavior. According to Figures 6(b), 6(e)–6(g), due to the friction and squeeze occlusion between rock blocks, the broken rock blocks of the lower key strata and the upper key strata in the hard roof are hinged to form a voussoir beam structure. As longwall face advances, the voussoir beam structure will fracture, which will cause the surrounding rock failure.

If only the lower voussoir beam structure fractures in Figure 8(a), the block $B_2$ does not act on the lower voussoir beam structure due to the hinge action of rock blocks in the upper key strata, and the limit fracture span of the lower voussoir beam structure is small, and it easily forms a small periodic weighting. The interaction force between lower key strata is ignored, and the dynamic loads $Q_{lv}$ bore by supports could be calculated as

$$Q_{\mathrm{lv}} = K_{\mathrm{dlv}} B \left\{ \sum_{i=1}^{j} P_i \left[ 2 - \frac{l_i \tan(\varphi_i - \alpha_i)}{2(h_i - \delta_i)} \right] + L_d h_d \gamma_m + + L_d h_z \gamma_z \right\}, \tag{8}$$

where $K_{\mathrm{dlv}}$ is the impact loads coefficient of the lower voussoir beam structure instability; $\delta_i$ is the sinking amount of the hinged rock block $B_1$ in the key strata of the lower voussoir beam structure, m; $\varphi_i$ is the friction angle between the hinged rock blocks of the $i^{\mathrm{th}}$ layer in the lower key strata; and $\alpha_i$ is the fracture angle of the rock.

The instability of lower voussoir beams may also cause upper voussoir beams instability, which will form serious small periodic weighting. In No. 8100 longwall face, the two key strata of No. 2 pebble conglomerate and No. 4 fine sandstone are simultaneously voussoir beam structure, the weighting interval is set as the limit fracture span of No. 2 pebble conglomerate, $l_1 = l_2 = 29.6$ m, $\varphi = 30^\circ$, $\delta$ is calculated as the compression amount of the rock based on bulking coefficient after the lower roof collapsed, and the other parameters remain unchanged; take $K_{dl} = 1.0$, and substitute the rock mechanical parameters in Table 1 into equation (8); then, $Q_l = 9851.51$ kN. When $K_{\mathrm{dl}} = 1.52$, $Q_l = 15000$ kN, namely, when $K_{\mathrm{dl}} > 1.52$, the simultaneous instability of voussoir beam structure in the lower key strata could cause the overburden loads to exceed the support working resistance, and it will cause a serious small periodic weighting when the lower voussoir beam structure fractures.

However, the voussoir beam structure is hinged between the rock blocks at the far-end of the goaf, and it has the restraining to the broken blocks behind the goaf. After the cantilever beam structure fracturing, there is more space for rotation behind the goaf, and there is no restrain of the broken blocks at its free end, which is different from the restrain of the broken blocks behind the voussoir beam structure. And only the top beam of the supports is completely pushed beyond the broken line of the cantilever beam structure, and supports could avoid the rotation movement of the broken blocks behind the longwall face. Compared with the lower cantilever beam structure, the limit fracture span of the lower voussoir beam structure is greater than or equal to the cantilever beam, and the free end of the cantilever beam may have a higher free-fall than the voussoir beam. The differences between them are the impact effect. Due to the magnitude of the load factor, both may generate severe underground pressure behavior, and the impact loads of the lower cantilever beam structure instability will be much greater than that of the lower voussoir beam structure.

When the upper voussoir beam structure is unstable, the block $B_2$ and the upper strata loads controlled by $B_2$ will act on the lower voussoir beam structure, as shown in Figure 8(b). They will drive the lower voussoir beam structure to lose stability. And the load $Q_v$ acting on the supports after the upper voussoir beam structure instability could be further calculated with the following equation:

$$Q_v = K_{\mathrm{dv}} B \left\{ \sum_{i=1}^{j} P_i \left[ 2 - \frac{l_i \tan(\varphi_i - \theta_i)}{2(h_i - \delta_i)} \right] + \left[ 2 - \frac{l_v \tan(\varphi - \alpha)}{2(h_{4v} - \delta_{4v})} \right] P_{4v} + L_d h_d \gamma_m + + L_d h_z \gamma_z \right\}, \tag{9}$$

where $K_{\mathrm{dv}}$ is the impact loads coefficient of the upper voussoir beam structure instability; $h_{4v}$ is the thickness of the key strata in the upper voussoir beam structure, m; $\delta_{4v}$ is the deflection of the hinged rock block $B_2$ in the key strata of the upper voussoir beam structure, m; $P_{4v}$ is the loads of the hinged rock blocks and the upper control rock strata in the key strata of the upper voussoir beam structure, kN.

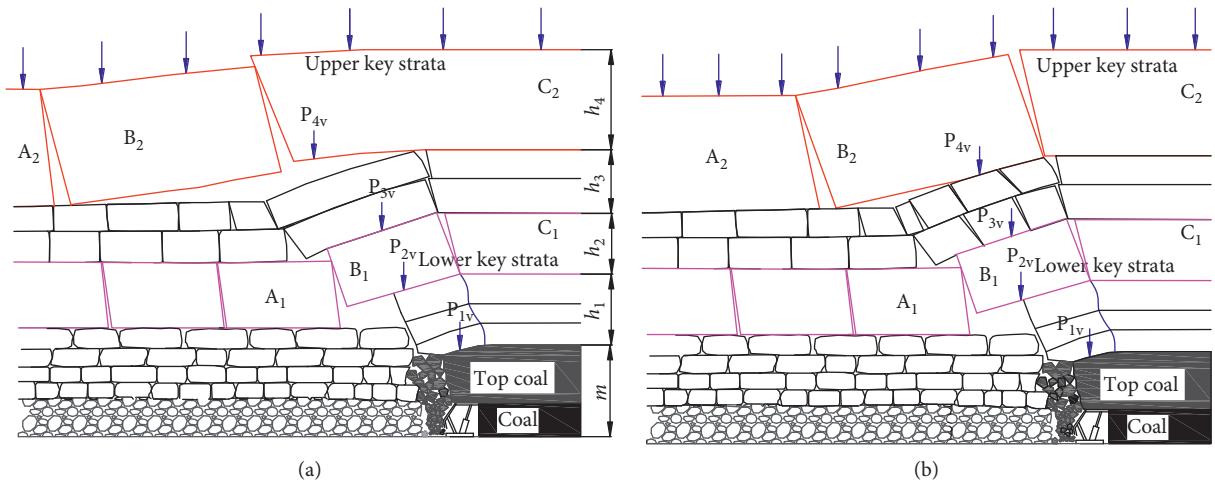


Figure 8: Modes of composite structure of lower and upper voussoir beam with hard main roof. (a) Instability of lower voussoir beam. (b) Synchronous instability of lower and upper beams.

Therefore, if $K_{dlv} = K_{dv}$, then $Q_v > Q_{lv}$. Since the lower voussoir beam structure only acts on the irregularly arranged gangue area in the goaf, it may prompt the lower key strata to slip or deform because of the bulking and the large compression deformation of the gangue. And it will result in serious underground pressure behavior. The instability of the upper voussoir beam will simultaneously drive the instability of the lower voussoir beam; then, the instability of the lower voussoir beam has the less loads than that of the upper voussoir beam.

According to calculation results, the ultimate fracture span of the upper key stratum in No. 8100 longwall face is larger than 37.2 m, the vertical distance between the key strata of No. 8 fine sandstone and No. 12 fine sandstone is 60 m, and it reaches up to 140 m between the key strata of No. 12 fine sandstone and No. 16 fine sandstone. If $\alpha = 70^\circ$, the maximum fracture span of the voussoir beam structure formed by the upper No. 12 key stratum is 21.84 m behind the No. 8 fine sandstone key stratum, and it is 50.96 m behind the No. 12 fine sandstone key stratum in the No.16 key stratum, which is further behind the upper key strata in the roof. Hence, the broken line of the voussoir beam structure formed by the No.12 key stratum is still in the range of the instability of the lower cantilever beam or the voussoir beam structure, and the broken line of the voussoir beam structure formed by the No. 16 key stratum is in the goaf far away from the lower structure fractures.

Therefore, the upper strata load controlled by the upper voussoir beam structure could only be calculated up to the upper No. 12 key stratum and its controlled upper loads. The thickness of itself and the loads strata has reached 140 m. If the loads of the supports are calculated with 8 times of mining height according to the empirical factor, the thickness of the loads strata is only 120 m, and the impact loads of the hard roof is not considered. Under the lower cantilever beam-upper voussoir beam structure or the lower and upper voussoir beam structures, the impact loads formed by their composite structures of the hard main roof is much higher than the empirical coefficient. And the working resistance of supports should be estimated based on the composite fracture structures formed by the hard main roof. Then, supports could also absorb and balance the dynamic loads of the main roof structure instability and its residual impact loads, and the failure of surrounding rock and supports crushing disasters in the longwall face will be avoided.

## 5. Hydraulic Fracture Technique for Modifying the Composite Structures

When the structural instability of the lower beam is caused by itself or the upper voussoir beam, it easily causes the surrounding rock damage or even the supports break-off. In order to control the dynamic loads of the main roof instability, the hydraulic fracture technologies were adopted in the No. 8105 LTCC face to change the hard main roof composite structures. The lower key strata are cut by hydraulic fracture technique to observe the weakening effect [27]. Then, they will prevent the instability of the hard main roof.

*5.1. Hydraulic Fracture Parameters.* The thickness of the hard roof in No. 8100 longwall face reaches about 11.4 m, the composite strata contain silty, fine, and gravel sandstone, and they are super thick layers and difficult to caving. Because it is difficult to carry out long-distance drilling onsite, the fractured rock strata are mainly filled with all the goaf after fracture and bulking, and the lower fine-grained sandstone layer was only fractured, with a total thickness of fracture about 22.25 m. Then, the dynamic loads induced by the lower cantilever beam or voussoir beam were weaken, and the instability of the lower cantilever beam or voussoir beam caused by the upper voussoir beam structure was alleviated. According to the self-weight stress principle, the fracturing water pressure was set as 42 MPa, the water injection pressure is not less than the ultimate tensile strength of coal and rock mass, and the water pressure will not be

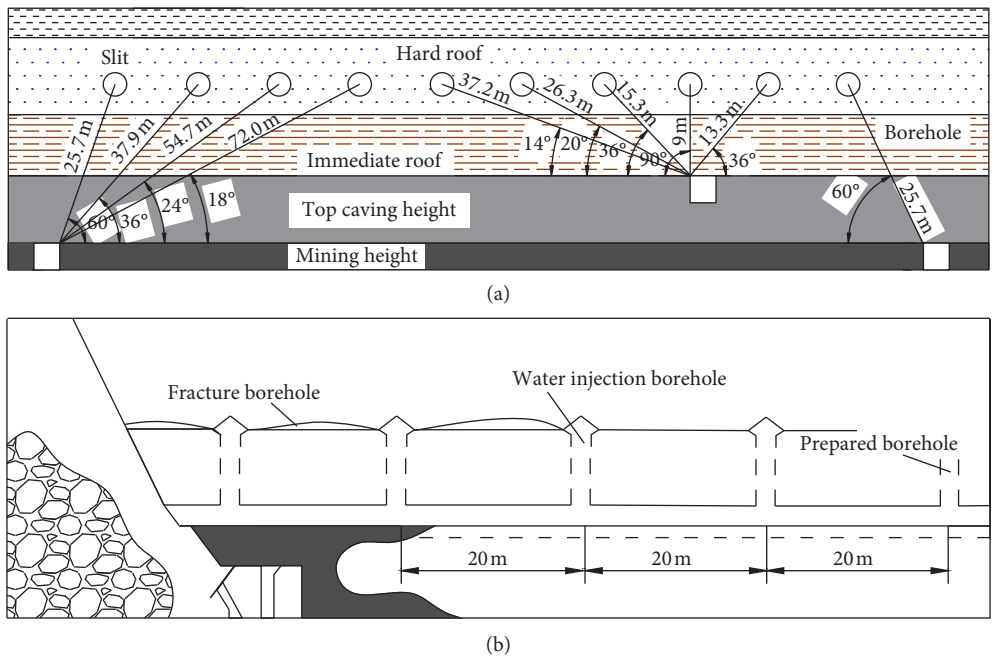


Figure 9: Layout of hydraulic cutting boreholes [27]. (a) Profile along the dip direction of the coal seam. (b) Profile along the strike of the coal seam.

Table 5: Comparison of underground pressure in the middle of No. 8105 and 8100 longwall face [27].

| Longwall face number | | 8100 | 8105 |
|---|---|---|---|
| Working resistance during weighting (kN) | Value distribution interval | 10000–14000 | 8000–13000 |
| | Average value | 12805.6 | 10895.7 |
| Periodic weighting interval/m | Value distribution interval | 11.48–44.6 | 9.6–36.6 |
| | Average value | 29.4 | 24.8 |

released from the cracks. The single borehole water injection volume was set as 0.8 $m^3$, and the single borehole water injection time was about 500 seconds. The borehole spacing could be determined according to the wetting radius of the water injection borehole, and it was set as 20 m.

*5.2. Boreholes Layout.* The hydraulic fracture was carried out in the top tailgate and the two gateways of the No. 8105 longwall face, and the construction was carried out in advance of mining. The test area was 200 m in length, and the distance along the strike and inclination of the face was both 20 m. A total of 10 drilling holes were designed for each row or group, 5 drill holes were drilled in the top tailgate, the water injection boreholes were set on both sides, 4 drill holes were drilled in the haulage roadway, and 1 drill hole was drilled in rail roadway. The boreholes layout and parameters are shown in Figure 9.

The borehole diameter was 44 mm, and the borehole depth was 9–72 m. The elevation angle of the boreholes depends on the drilling site and the position of the water injection. The maximum elevation angle was 90° and the minimum was 18°. The initial hydraulic pressure was 50 MPa, and the initial fracture borehole diameter was 75 mm. And they were used to presplit the difficulty caving of main roof in advance of longwall face.

*5.3. Weakening Effect of Hydraulic Cutting on Reducing Roof Pressure.* In No. 8105 longwall face, the water pressure remained at 35 MPa for the 1# borehole during the high-pressure water injection. After setting the protection pressure of the pumping station to 56 MPa, the water pressure instantly increased to 46.22 MPa, and then, the fracture began. As the borehole cracks opened and flushed alternately, the water pressure in the boreholes show a "rising-falling-rising" trend.

After hydraulic cutting, the weighting interval in No. 8105 face was 9.6–36.6 m, with an average of 24.8 m. The No. 8100 and No. 8105 longwall face are in the same panel area, the geological conditions of the surrounding rock are basically the same as the production technical conditions, while the No. 8100 face has not taken the weakening measures. Table 5 provides the comparison of support working resistance and weighting interval in the middle of No. 8100 and No. 8105 longwall face.

According to Table 5, the weighting interval and the working resistance in the No. 8105 and No. 8100 longwall

face have a significant difference. After hydraulic cutting, the minimum weighting interval in the No. 8105 longwall face was reduced by 1.88 m compared with No. 8100 face, the maximum weighting interval was reduced by 11 m, and the impact loads after periodic weighting was significantly reduced, the average weighting interval had been reduced by 4.6 m. During the periodic weighting, the minimum working resistance of supports was 8000 kN in No. 8105 longwall face, which was reduced by about 20.0% compared with No. 8100 longwall face; the maximum working resistance was also reduced by 1000 kN and about 7.1%, and the average was reduced by about 8.8%. Hence, the hydraulic cutting reduces the working resistance of the supports and weighting interval, which could control the instability of the lower cantilever beam or voussoir beam induced by the upper voussoir beam structure. Therefore, the hydraulic cutting could improve the mining efficiency of the LTCC face with large mining height and hard main roof.

## 6. Conclusion

In this study, the weighting interval and underground pressure behaviors of the hard main roof in LTCC face with large mining height were monitored on the site. The fracture patterns of roof and coal samples were obtained under the uniaxial compression, and the composite structures induced by hard main roof fracture in LTCC face with large mining height were studied by the two-dimensional similar material test. Based on the key stratum theory, the fracture composite characteristics and its stability of hard main roof were analyzed. And the hydraulic fracturing technology was proposed to weaken the weighting interval and dynamic loads in LTCC face. The main conclusions are as follows:

(1) As the LTCC face with large mining height advances, the hard main roof weighting interval presents obvious long and short period nesting effects. Under the uniaxial compression, the coal in No. 8100 longwall face mainly occurs as split failure, and the hard roof occurs as shear failure; after the coal and roof reach the peak value of uniaxial stress, it immediately decreases to residual strength. Under the overburden loads, the top coal and roof strata tend to instantaneous fracture and instability, which will have an impact on the coal rib and supports.

(2) The position of broken line in LTCC face with large mining height could be summarized as three cases: in front of the supports, just above the supports, and lagging the supports; the hard main roof fracture structures are summarized as two types: lower cantilever beam-upper voussoir beam and lower voussoir beam-upper voussoir beam. And the damage of surrounding rock depends on the fracture structure of hard main roof and the position of the broken line.

(3) Two composite structures mechanical models of hard roof fracture are built and used to evaluate the stability of overburden strata, respectively, and the support loads could be calculated with different mechanical models of composite fracture structures.

## Data Availability

The data used to support the findings of this study are included within the article.

## Conflicts of Interest

The authors declare that they have no conflicts of interest.

## Acknowledgments

This work was supported by the National Natural Science Foundation of China (51904303), the Ministry of Science and Technology of China (2018YFC0604501), and Fundamental Research Funds for the Central Universities (2020YJSNY14).

## References

[1] J. Emery, I. Canbulat, and C. Zhang, "Fundamentals of modern ground control management in Australian underground coal mines," *International Journal of Mining Science and Technology*, vol. 30, no. 5, pp. 573–582, 2020.

[2] R. Gao, T. Kuang, Y. Zhang, W. Zhang, and C. Quan, "Controlling mine pressure by subjecting high-level hard rock strata to ground fracturing," *International Journal of Coal Science & Technology*, vol. 8, 2021.

[3] Z. Song, K. Heinz, and H. Martin, "Drawing mechanism of fractured top coal in longwall top coal caving," *International Journal of Rock Mechanics and Mining Sciences*, vol. 130, pp. 1–13, 2020.

[4] D. Le Tien, R. Mitra, and J. Oh, "A review of roof instabilities associated with longwall top coal caving," in *Proceedings of the 52nd U.S. Rock Mechanics/Geomechanics Symposium*, American Rock Mechanics Association, Seattle, WA, USA, June 2018.

[5] G. Zhang, C. Zang, M. Chen et al., "Ground response of entries driven adjacent to a retreating longwall panel," *International Journal of Rock Mechanics and Mining Sciences*, vol. 138, 2021.

[6] G. C. Zhang, Z. J. Wen, S. J. Liang et al., "Ground response of a gob-side entry in a longwall panel extracting 17 m-thick coal seam: a case study," *Rock Mechanics and Rock Engineering*, vol. 53, no. 2, pp. 497–516, 2020.

[7] F. Du, K. Wang, X. Zhang, C. Xin, L. Shu, and G. Wang, "Experimental study of coal-gas outburst: insights from coal-rock structure, gas pressure and adsorptivity," *Natural Resources Research*, vol. 29, no. 4, pp. 2481–2493, 2020.

[8] L. Yu and S. Yan, "The basic principle of roof strata control in fully mechanized caving mining of extra thick coal seam," *Journal of the China Coal Society*, vol. 45, pp. 31–37, 2020.

[9] S. Yan, X. Yin, and H. Xu, "Roof structure of short cantilever-articulated rock beam and calculation of support resistance in full-mechanized face with large mining height," *Journal of the China Coal Society*, vol. 36, no. 11, pp. 1816–1820, 2011.

[10] H. Li, D. Jiang, and D. Li, "Analysis of ground pressure and roof movement in fully-mechanized top coal caving with large mining height in ultra-thick seam," *Journal of the China Coal Society*, vol. 39, no. 10, pp. 1956–1960, 2014.

[11] J. Ju and J. Xu, "Structural characteristics of key strata and strata behaviour of a fully mechanized longwall face with 7.0 m height chocks," *International Journal of Rock Mechanics and Mining Sciences*, vol. 58, pp. 46–54, 2013.
[12] B. Yu, J. Zhao, T. Kuang, and X. Meng, "In situ investigations into overburden failures of a super-thick coal seam for longwall top coal caving," *International Journal of Rock Mechanics and Mining Sciences*, vol. 78, pp. 155–162, 2015.
[13] J. Xu, "Strata control and scientific coal mining—a celebration of the academic thoughts and achievements of Academician Minggao Qian," *Journal of Mining and Safety Engineering*, vol. 36, no. 1, pp. 1–6, 2019.
[14] H. Wang, X. Fang, F. Du et al., "Three-dimensional distribution and oxidation degree analysis of coal gangue dump fire area: a case study," *Science of the Total Environment*, vol. 772, Article ID 145606, 2021.
[15] H. Wang, B. Tan, Z. Shao, Y. Guo, Z. Zhang, and C. Xu, "Influence of different content of $FeS_2$ on spontaneous combustion characteristics of coal," *Fuel*, vol. 288, p. 119582, 2021.
[16] J. Xu and M. Qian, "Study on the influence of key strata movement on subsidence," *Journal of China Coal Society*, vol. 25, no. 2, pp. 122–126, 2000.
[17] M. Qian and J. Xu, "Behaviors of strata movement in coal mining," *Journal of the China Coal Society*, vol. 44, no. 4, pp. 973–984, 2019.
[18] J. Zhou and Q. Huang, "Stability analysis of key stratum structures of large mining height longwall face in shallow coal seam," *Chinese Journal of Rock Mechanics and Engineering*, vol. 38, no. 7, pp. 1396–1407, 2019.
[19] B. Unver and N. E. Yasitli, "Modelling of strata movement with a special reference to caving mechanism in thick seam coal mining," *International Journal of Coal Geology*, vol. 66, no. 4, pp. 227–252, 2006.
[20] G. S. Esterhuizen, D. F. Gearhart, and I. B. Tulu, "Analysis of monitored ground support and rock mass response in a longwall tailgate entry," *International Journal of Mining Science and Technology*, vol. 28, no. 1, pp. 43–51, 2018.
[21] Z. Li, S. Zhang, and F. Du, "Novel experimental model to investigate fluid-solid coupling in coal seam floor for water inrush," *Technical Gazette*, vol. 25, no. 1, pp. 216–223, 2017.
[22] J. Liu, C. Dong, S. Zhang, and Y. Zhang, "Research on the rules of overlying rock movement by similar material simulation in fully mechanized top coal caving mining with high cutting height," *Applied Mechanics and Materials*, vol. 522–524, pp. 1419–1425, 2014.
[23] L. Huo, *Study on the Height of Caving Zone in Fully Mechanized Top Coal Caving with Large Mining Height*, China university of Mining & Technology (Beijing), Beijing, China, 2014.
[24] M. Qian, X. Miu, and J. Xu, *Key Strata Theory in Ground Control*, China University of Mining & Technology Press, Xuzhou, China, 2000, in Chinese.
[25] L. Yu, S. Yan, and Q. Liu, "Determination of support working resistance of top coal caving in extra thick coal seam," *Journal of China Coal Society*, vol. 37, no. 5, pp. 737–742, 2012.
[26] J. Xu and J. Ju, "Structural morphology of key stratum and its influence on strata behaviors in fully-mechanized face with super-large mining height," *Chinese Journal of Rock Mechanics and Engineering*, vol. 30, no. 8, pp. 1547–1556, 2011.
[27] A. Wang, "Hydraulic fracturing technology for extremely thick coal seam with hard roof in Tongxin mine," *Safety in Coal Mines*, vol. 46, no. 3, pp. 54–57, 2015.